Structure of hibernating ribosomes studied by cryoelectron tomography in vitro and in situ

Structure of hibernating ribosomes studied by cryoelectron tomography in vitro and in situ

Julio O. Ortiz,[1] Florian Brandt,[1] Valério R.F. Matias,[1] Lau Sennels,[3] Juri Rappsilber,[3] Sjors H.W. Scheres,[4] Matthias Eibauer,[1] F. Ulrich Hartl,[2] and Wolfgang Baumeister[1]

[1]Department of Molecular Structural Biology and [2]Department of Cellular Biochemistry, Max Planck Institute of Biochemistry, Martinsried 82152, Germany
[3]Wellcome Trust Centre for Cell Biology, University of Edinburgh, Edinburgh EH9 3JR, Scotland, UK
[4]Biocomputing Unit, Centro Nacional de Biotecnología (CSIC), Cantoblanco, 28049 Madrid, Spain

Ribosomes arranged in pairs (100S) have been related with nutritional stress response and are believed to represent a "hibernation state." Several proteins have been identified that are associated with 100S ribosomes but their spatial organization has hitherto not been characterized. We have used cryoelectron tomography to reveal the three-dimensional configuration of 100S ribosomes isolated from starved *Escherichia coli* cells and we have described their mode of interaction. In situ studies with intact *E. coli* cells allowed us to demonstrate that 100S ribosomes do exist in vivo and represent an easily reversible state of quiescence; they readily vanish when the growth medium is replenished.

Introduction

An early description of *E. coli* 70S ribosomes reported that these particles were frequently found associated in pairs, later referred to as 100S ribosomes (Tissieres and Watson, 1958). It was subsequently observed that the formation of 100S ribosomes occurs in stationary phase (Wada, 1998). The 100S ribosomes are distinct from disomes (two ribosomes linked by mRNA) in that they are not translationally active, but represent a storage form or hibernation state (Wada et al., 1995). The ribosome modulation factor (RMF), and the hibernation promoting factor (HPF, previously known as YhbH), are known to be involved in the formation and maturation of these ribosome dimers, respectively, whereas YfiA (protein Y) is suggested to bind 70S ribosomes in stationary phase (Wada et al., 1990; Maki et al., 2000). Some aspects of the interaction of these factors with the translational machinery have been explored in recent years (Ueta et al., 2005, 2008; Yoshida et al., 2009), but the interpretation of these data has been hampered by the lack of a detailed 3D structure of 100S ribosomes.

Correspondence to Wolfgang Baumeister: baumeist@biochem.mpg.de

S.H.W. Scheres' present address is MRC Laboratory of Molecular Biology, Hills Road, Cambridge CB2 0QH, England, UK.

Abbreviations used in this paper: CCF, cross-correlation function; CET, cryoelectron tomography; CTF, contrast transfer function; f-f, ribosomal arrangement as "front-to-front"; HPF, hibernation promoting factor; IF3, initiation factor 3; (p)ppGpp, guanosine pentaphosphate or tetraphosphate; RMF, ribosome modulation factor; RRF, ribosome recycling factor; t-t, ribosomal arrangement as "top-to-top".

X-ray crystallography and EM single-particle analysis have provided unprecedented insights into the molecular architecture of ribosomes and have been instrumental in elucidating key events during translation (for review see Schmeing and Ramakrishnan, 2009). Both techniques rely, more or less, on homogeneous samples of ribosomes, ideally trapped in a particular functional state. Other higher-order structures, such as polysomes, display a degree of plasticity in their supramolecular organization, which makes them intractable to x-ray crystallography or single-particle analysis. Cryoelectron tomography (CET; Lučić et al., 2005) can complement these techniques by allowing the visualization of variable or flexible molecular structures both in vitro and in situ (Ortiz et al., 2006), i.e., in the functional environment of intact cells. Although the resolution is considerably lower than that achieved by x-ray and single-particle cryo-EM, computational analysis of subtomogram volumes opens the way for hybrid approaches to interpret the tomograms in the light of preexisting high resolution structures. In the past, we have used such an approach to study the native 3D organization of *E. coli* ribosomes in densely packed polysomes (Brandt et al., 2009). Here, we report a structural study of ribosomal dimers (100S) by CET, both in ribosome-enriched fractions from starved *E. coli* cells and in intact cells cultured in minimal medium.

The Rockefeller University Press $30.00
J. Cell Biol. Vol. 190 No. 4 613–621
www.jcb.org/cgi/doi/10.1083/jcb.201005007

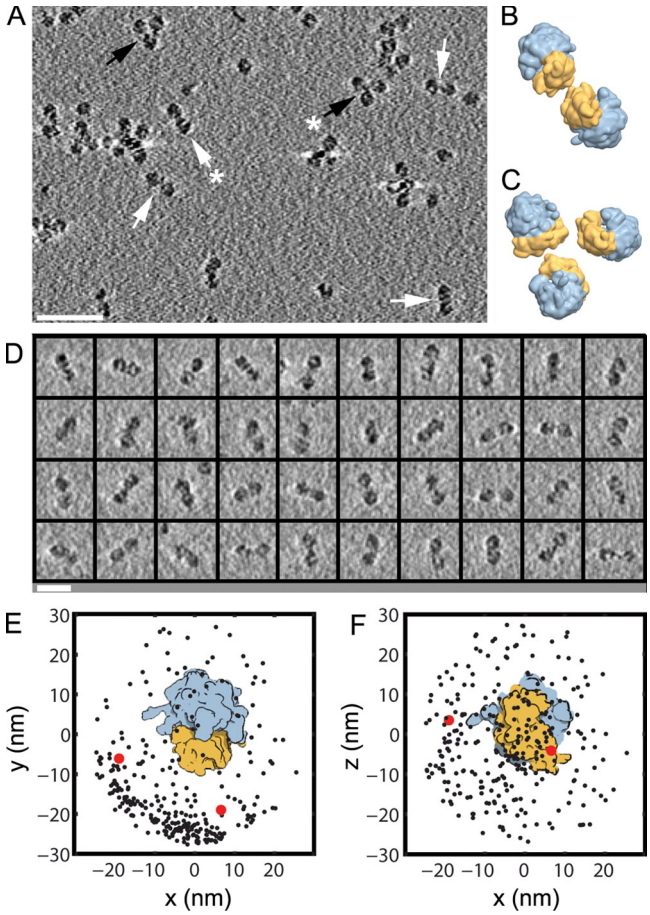

Figure 1. **Variability in the spatial relationship of identified ribosomes within tomograms of starved *E. coli* lysates.** (A) XY slice of tomogram (bar, 100 nm). White arrows indicate 100S particles and black arrows ribosomal trimers. Isosurfaces of a reference ribosome (30S, yellow; 50S, blue) were placed in relative orientations found by template matching for the examples of a dimer (B) and a trimer (C) indicated by asterisks in A. (D) Gallery of representative 100S particles detected in different tomograms (bar, 50 nm). (E and F) Center-to-center 3D distance vectors (black dots) between each ribosome and its next neighbor, depicted by x-y and x-z plots. The plot corresponds to the subset of 271 ribosomes with one or more ribosomal neighbors from 1,232 identified ribosomes. Red dots represent the centers of clusters observed in densely packed polysomes (Brandt et al., 2009).

Results

Variability of isolated ribosomal assemblies

Initially, 100S ribosomes were investigated in vitro, i.e., in diluted cell lysates in which nonspecific interactions are reduced. Cell lysates can be examined in relative thin (~50–200 nm) ice layers compared with the much thicker ice layers (>0.5 µm) needed for embedding cellular structures. The thicker ice layers result in a degradation of image quality. Tomograms were acquired from frozen-hydrated samples derived from *E. coli* cells grown to starvation in which clusters of ribosomes with a variable number of 70S particles could be observed (Fig. 1 A). Visual inspection of the tomograms showed that 20–25% of the 70S ribosomes formed dimers (Fig. 1 D), which associate via their small subunits (30S), in agreement with earlier 2D studies of stained samples (Wada, 1998; Yoshida et al., 2002). This number might well be an underestimate of the abundance of 100S ribosomes, given the fact that the 100S particles easily dissociate into monomeric ribosomes. The remaining ribosomal particles were individual 70S ribosomes or clusters of three or more ribosomes in close proximity. The ribosomes forming trimers also appeared to associate via the 30S subunits.

We performed a 3D analysis of the tomographic data using template matching for an initial determination of the relative positions and orientations of the 70S ribosomes (Frangakis et al., 2002). A reference density map derived from the crystal structure of an *E. coli* ribosome (Schuwirth et al., 2005) was used as a template to detect and align individual ribosomes (Fig. S1). Replacement of individual ribosomes by the template in the orientation determined for the given ribosomes confirmed the proximity of small ribosomal subunits (Fig. 1, B and C). The position and orientations determined by template matching were used for the 3D analysis of center-to-center vector distances between neighboring ribosomes. This analysis provided an objective characterization of the spatial organization of ribosomes. The two 30S subunits of each dimer are in close proximity, but their relative orientation is more variable than in stalled polysomes where the densely packed ribosomes are found in two clearly preferred relative orientations (Fig. 1, E and F; Brandt et al., 2009). The association of ribosome pairs isolated from starving cells seems to have a higher degree of translational and rotational freedom around the contact sites, which are located between the entry and exit sites of the mRNA on the 30S subunits. We determined an average center-to-center spacing of 25.6 nm for neighboring ribosomes in the tomograms of starved cell lysates, a larger separation than the 21.6 nm found previously with stalled polysomes (Brandt et al., 2009).

When all the subtomograms containing monomeric, dimeric, as well as trimeric ribosomes were aligned with a 70S ribosome reference and averaged, the resulting density map showed a 70S particle with some additional blurred density around the 30S subunit, but no well-defined density corresponding to a second 70S particle as would be expected for a rigid and well-defined ensemble (Fig. 2 A). But this is not surprising given the low abundance of dimeric ribosomes in the sample (see above) and the flexible nature of the linkage between monomers, discernible already in the raw data.

To verify the identification of ribosomes in selected subtomograms and their correct localization in 3D space, a subset of subtomograms was aligned in a completely unsupervised manner using a novel, reference-free maximum-likelihood refinement algorithm for 3D images with missing data regions in Fourier space (Scheres et al., 2009). The refined model was almost indistinguishable from the one obtained using alignment based on template matching (Fig. 2 F). The similarity between the models proves that the use of a reference in the template-based approach does not introduce a bias in this case.

Next, we applied successive steps of classification to the data using constrained correlation (Förster et al., 2008; Fig. 2, B–E). Dimer-only class averages created from independent sample pools clearly showed density for both 70S particles (Fig. 2, C and D). It was reassuring to see that the result obtained with template matching and the nonsupervised alignment and

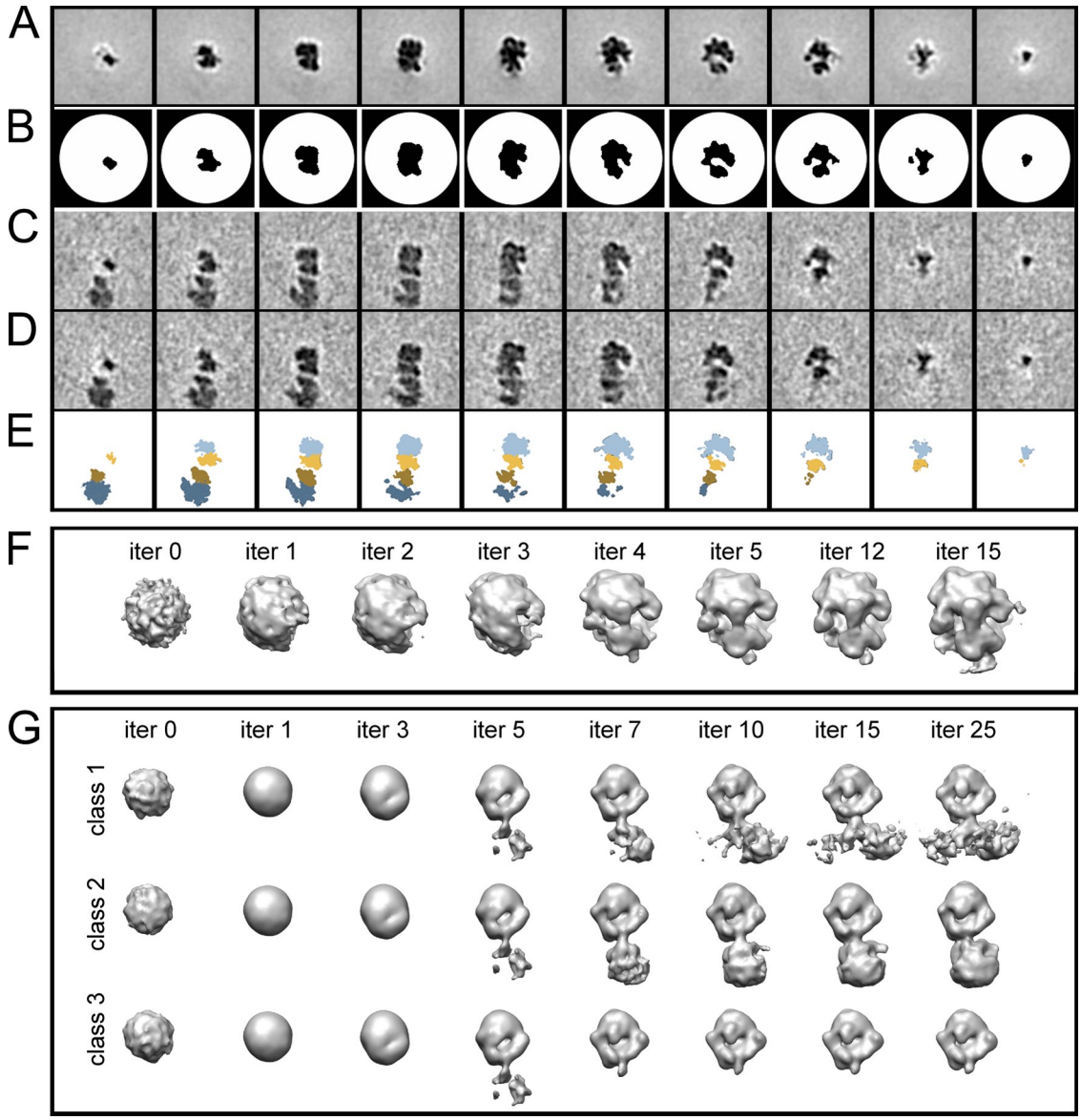

Figure 2. **Alignment and classification of identified ribosomes in tomograms from starved *E. coli* lysates.** (A–E) Reference-based alignment and classification using constrained correlation. (A) Slices of the average structure derived from 1,232 subtomograms (Pool II) containing 70S ribosomes. (B) Mask used for classification excluding the aligned central ribosome. (C and D) Slices of average structures containing 100S ribosomes with the two ribosomes in a preferred orientation derived from 43 classified subtomograms from Pool II and 35 classified subtomograms from Pool I, respectively. (E) Schematic slices of the two ribosomes oriented as in C (50S, blue; 30S, yellow; light colors for central ribosome excluded during classification; dark colors adjacent particle revealed after classification). (F and G) Unsupervised alignment and classification using a maximum likelihood approach. (F) Isosurface representation of 3D maps obtained during iterative reference-free alignment of 601 subtomograms (Pool I) that were windowed to contain only a single ribosome particle. Iteration 0 (iter 0) corresponds to the initial, unbiased reference that was obtained by averaging over all sub-tomograms in random orientations. The final map (iter 15) has a resolution of 38 Å according to the FSC = 0.5 criterion and is readily identified as a 70S ribosome particle. (G) Simultaneous alignment and classification of the same particles used in F, but without windowing in order to include neighboring ribosomes. Three initial reference structures (class 1–3, iter 0) were refined simultaneously during 25 iterations. Note that during the first 5 iterations similarity between the three references was imposed. The final averages (iter 25) were interpreted as class 1 trimers (or larger clusters, 74 particles), class 2 dimers (158 particles), and class 3 monomers of 70S ribosome (369 particles).

classification yielded very similar results (Fig. 2 G; Fig. S4). The dimers have an approximate twofold symmetry axis. However, differences in the composition and conformation of the ribosomal subunits in each dimer that may exist as some variability in the 3D averages were observed depending on which monosome from each pair was aligned to the reference (nonredundant averages). Thus, an unambiguous assignment of each ribosome in a pair to a position in the dimer was not possible.

In a 70S ribosome, the surface of the 30S subunit that is opposed to the inter-subunit space is commonly referred to as the cytosolic face (Fig. S1, "front" view). In the refined structure of the 100S ribosome, the cytosolic faces of the two 30S subunits are juxtaposed (Fig. 3 A). We denote this arrangement as "front-to-front" (f-f; Fig. 3 B). The pairing in the structure derived from hibernating ribosomes is quite different from the one found in stalled polysomes in vitro, called "top-to-top" (t-t; Fig. 3 B).

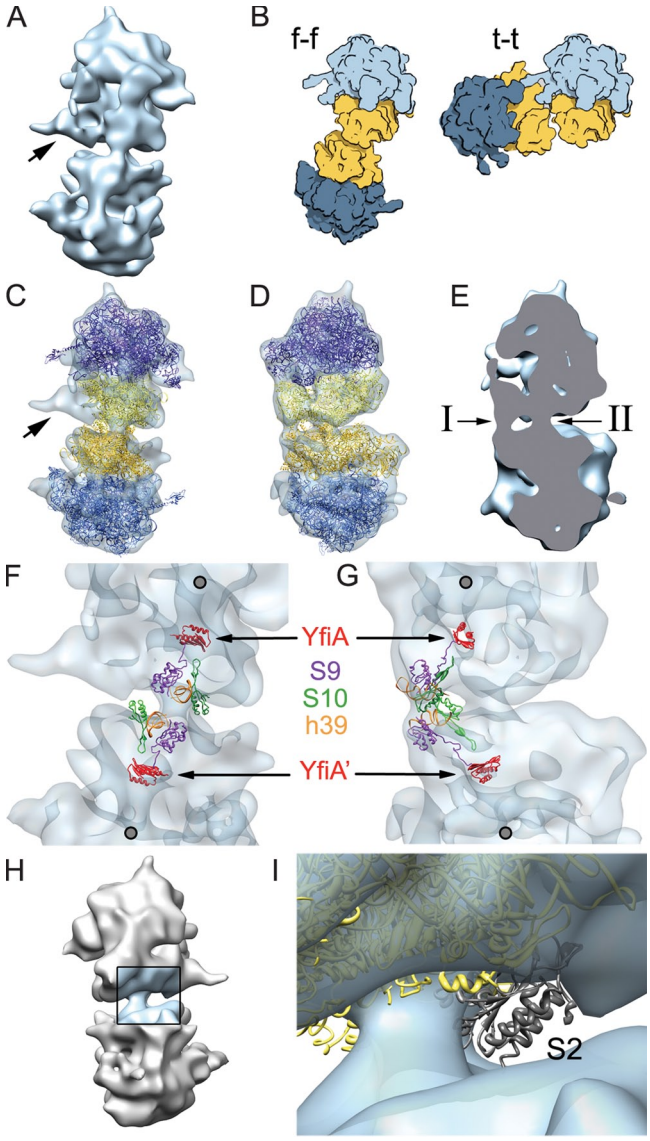

Figure 3. **Interaction regions between small subunits of the 100S ribosome.** (A) "Top" view of the averaged 100S ribosome density map. (B) Schematic representation of large (blue) and small (yellow) subunits in the f-f ribosomal arrangement found in starvation conditions, and the t-t organization characteristic for stalled polysomes. (C and D) Docking of 70S ribosome crystal structure (Schuwirth et al., 2005) into the two ribosomal particles of the 100S ribosome map in "top" and "right" views, respectively. An unassigned density protrudes close to the exit of the mRNA tunnel (A and C, arrows). (E) Two major contact regions between the ribosomes in the 100S particles are conspicuous in a longitudinal cut the map in the "right" view (I and II). Docking of the YfiA–70S ribosome complex (Vila-Sanjurjo et al., 2004) into the 100S density map suggests that proteins S9, S10, and helix 39 of the 16S rRNA are in the contact region I (F and G, "top" and "right" view, respectively). S9 and S10 have domains which extend toward the YfiA binding site. The suggested ribosomal binding sites for RMF are also indicated (gray dots; Yoshida et al., 2002, 2004). (H) "Bottom" view of the 100S ribosome density map with contact region II highlighted in blue. (I) In the docked 70S ribosome crystal structure (Schuwirth et al., 2005), protein S2 is located outside the map envelop adjacent to the contact region II (view corresponds to detail in H).

In tightly packed polysomes, the t-t organization minimizes the distance between the mRNA tunnel exit of one ribosome and the mRNA entry of the neighbor at the 5′ end of the messenger (Brandt et al., 2009).

Rigid-body docking of two copies of the *E. coli* 70S ribosome structure into the dimer density map revealed possible interacting ribosomal components (Fig. 3, C and D). Two major contact regions between the small subunits of the dimers could be distinguished (Fig. 3 E). The first (I) involves proteins S9, S10, and the 16S rRNA helix 39 (Fig. 3, F and G). The second region (II) appears to involve the S2 protein because this protein is localized in the docked crystal structure adjacent to the density in the region II and it was found outside the density map envelope (Fig. 3, H and I). It has been suggested that S2 contacts the mRNA during movements associated with translation, and therefore displays a high degree of flexibility (Yusupova et al., 2006).

The f-f dimer average has additional density corresponding to a mass of approximately 25 kD associated with the small ribosomal subunit, in a region close to the mRNA tunnel exit and the so-called platform (Fig. 3, A and C). At the present resolution, it was not possible to assign any of the factors reported as being associated with 100S ribosomes, such as RMF (6 kD) and HPF (10.8 kD), unambiguously to these densities. It is in fact unlikely that the additional density associated with the 30S subunit is due to these factors. RMF has been shown to bind the large ribosomal subunit (50S) in a region close to the peptidyl transference center (Yoshida et al., 2002, 2004; Fig. 3, F and G). HPF shares 40% sequence homology with YfiA (12.7 kD; Ueta et al., 2005) and adopts an overall structure similar to YfiA (Sato et al., 2009). HPF has been suggested to bind to the peptidyl-tRNA site (P-site) and aminoacyl-tRNA site (A-site) of the 30S subunit, similar to where YfiA is known to dock (Vila-Sanjurjo et al., 2004; Fig. 3, F and G).

Additional proteins associated with 100S ribosomes

In an attempt to identify additional nonribosomal proteins bound to dimers, we analyzed crude ribosomal fractions isolated from starved *E. coli* by mass spectroscopy. Several candidate proteins were detected, including RMF, HPF, and YfiA, and several other ribosome-binding proteins, such as the stationary phase–induced ribosome-associated protein (SRA, 5 kD), the ribosome-dependent endonuclease RelE, and initiation and elongation factors (Table S1). At this stage, we have not yet been able to discriminate between factors that associate with 100S ribosomes, but not with 70S ribosomes, nor could we assign any of the candidate proteins to the extra density found on the 30S subunits. Future studies with tagged ribosomes allowing for a better purification and cross-linking approaches in conjunction with mass spectrometry should enable us to identify specific interactors and correlate them with the observed density.

Consistent with the suggested function of HPF in blocking tRNA binding in the A- and P-sites, we have not found densities in the canonical tRNA positions, even at low intensity thresholds. Given that the platform has been described as a center for translational regulation (Marzi et al., 2007), we consider a potential participation of structured mRNAs or other RNA molecules in the 30S-associated density present in the 100S ribosomes.

While this manuscript was under revision, Kato et al. (2010) published an article describing the structure of isolated

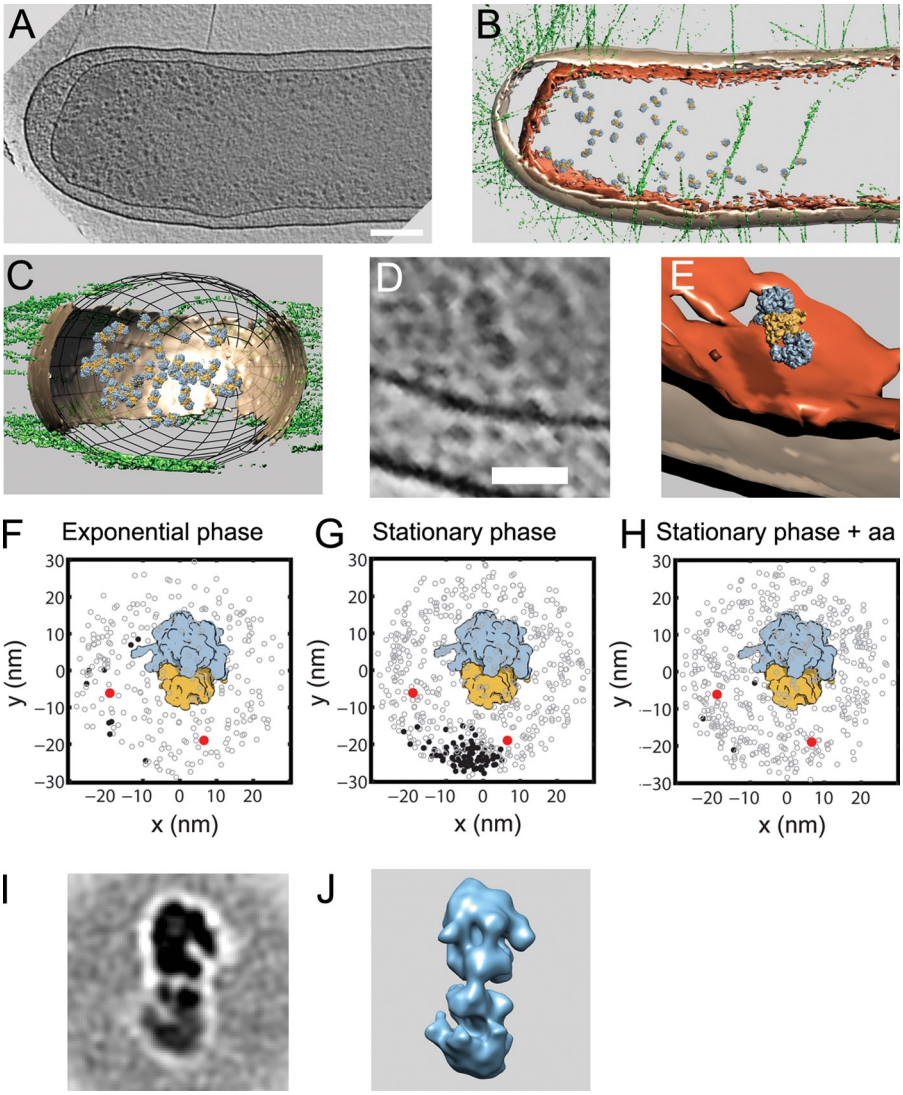

Figure 4. **100S Ribosomes identified in situ.** (A) Slice of a tomogram of an intact *E. coli* cell grown in minimal media (bar, 100 nm). Longitudinal (B) and transversal (C) views of corresponding isosurface representation. Models of 70S ribosomes with colored 30S (yellow) and 50S subunits (blue) are positioned where ribosome dimers were detected. The inner and outer membranes were manually segmented (dark and light brown, respectively), and were the basis of a membrane model (black grid). Manually segmented Pili are depicted in green. (D) A magnified tomographic section through a single ribosome dimer. (E) Surface rendering of a model ribosome dimer replacing the ribosomes shown in D (bar, 50 nm). (F–H) x-y plots of center-to-center 3D distance vectors between each ribosome and its closest ribosome neighbor. Plots correspond to representative tomograms for three different growth conditions: exponential phase (F), stationary phase (G), and grown to stationary phase but supplemented with amino acids (H). Filled dots correspond to particles clustered based on center-to-center vectors and relative orientations, circles represent single ribosomes. Only in stationary phase can a distinct cluster be observed. Two ribosome copies are clearly distinguishable in an XY slice (I) and the isosurface representation of an average of 878 subvolumes containing ribosome dimers extracted from tomograms of *E. coli* in stationary phase (J).

E. coli 100S ribosomes. They used cryo-EM in conjunction with single-particle analysis to generate a structural model. To reduce the risk of dissociation of the 100S particles into monomeric 70S particles they applied a mild chemical fixation and to cope with the flexible linkage between the two monomers the alignment was restricted to only one of them but including the small subunit of the adjacent monomer. This allowed them to determine the relative orientation of the monomers and to generate a synthetic 100S model from the individually reconstructed 70S particles. Despite of the different approaches taken (electro tomography vs. single-particle analysis), the resulting structures are in good agreement: the monomers interact flexibly via the 30S subunits and this interaction appears to involve protein S2; an additional mass not present in individual 70S particles was observed on the 30S subunits of the 100S ribosomes, but no density attributable to tRNAs was found.

Existence of 100S ribosomes in situ

The existence of ribosome dimers in vivo has remained a controversial issue because it cannot be ruled out that the ionic conditions of the working buffer could favor nonspecific interactions. Thus, we aimed at identifying 100S particles in situ by CET of intact *E. coli*. Cells grown in rich media have an average diameter of ~1 μm, which is too thick for a reliable identification of most macromolecules. Slow growth in minimal medium results in cells with a diameter of ~400 nm (Woldringh et al., 1977), improving tomogram quality significantly and thereby facilitating the recognition of macromolecular complexes. We recorded tomograms of *E. coli* cells grown in minimal media up to mid-exponential and stationary phases (Fig. 4, A–E) and analyzed the resulting ribosome distribution (Fig. 4, F–G; Fig. S2). We found that only cells grown to stationary phase have a fraction (10–20%) of identified ribosomes with neighboring 70S particles in the spatial arrangement described above as characteristic for 100S ribosomes (Fig. 4 G vs. Fig. 1 E). Interestingly, the clustering found in the cellular tomograms is indicative of a lower degree of variability in the relative orientation of the two monomers of the 100S ribosome in situ than in the in vitro preparations. Shear forces acting upon the particles during isolation might well cause distortions of the weakly connected monomers. Under conditions of exponential growth in minimal media we observed neither clustering indicative of dimers nor of

polysomes (Fig. 4 F), possibly because initiation events are rare under these conditions. It is known that the inhibition of ribosomes by RMF and consequent ribosome dimerization is reversible, as the 100S ribosomes dissociate back into 70S ribosomes within 2 min upon transfer of starved cells into fresh media (Wada et al., 1990; Yoshida et al., 2002). We tested whether the ribosomal clustering observed in stationary phase would vanish when supplying fresh nutrients. Indeed, no clustering of ribosomes was detected when cells previously grown to stationary phase in minimal media were supplemented with amino acids or transferred to rich media (Fig. 4 H). Moreover, a low resolution model of the f-f ribosome dimer was generated by averaging a subset of 70S ribosomes from tomograms of cells in stationary phase identified by classification as having a second ribosome attached (Fig. 4, I and J). The results confirm the physiological relevance of the f-f ribosome dimers observed in fractions from cell lysates and further support their association with nutritional stress.

Discussion

Our understanding of ribosomal clustering coupled to growth-phase transitions is summarized in Fig. 5. Stalling of ribosomes during translation is not unusual, and it can be caused, among other reasons, by secondary mRNA structures, rare codons, or amino acid scarcity (Buchan and Stansfield, 2007). Stalled ribosomes can be recycled by at least two different mechanisms: in the case of truncated messengers, by the tmRNA system or in the case of ribosomes stalled at the stage of elongation, by the initiation factor 3 (IF3) and the ribosome recycling factor (RRF; Singh et al., 2008). The synthesis of stable RNA species in many *E. coli* strains is sharply decreased by deprivation of amino acids. This response is predominantly regulated by the guanosine pentaphosphate or tetraphosphate [(p)ppGpp]. The level of (p)ppGpp in bacteria is controlled by two ppGpp synthetases (PSI/PSII), encoded by the relA and spoT genes (Murray and Bremer, 1996). The binding of uncharged tRNAs to the ribosomes is a signal for activation of the ribosome-bound PSI. The accumulation of (p)ppGpp reduces the synthesis of additional ribosomes and thereby reduces the consumption of amino acids; this in turn allows the remaining ribosomes to function at a higher rate (Bremer and Dennis, 2008). The transcription of the *rmf* gene is positively regulated by (p)ppGpp (Izutsu et al., 2001).

The inhibition of translation by ribosome–dimer formation during starvation has been attributed primarily to RMF binding, although the role of the RMF in the dimerization process is not yet well understood. The action of RMF might resemble the inhibition of translation by certain antibiotics (Yoshida et al., 2002). In more recent studies, it has been suggested that RMF promotes the formation of a 90S complex, which matures with the addition of HPF to form the 100S particle (Fig. 5, C and D; Ueta et al., 2005). Interestingly, the proteins S9 and S10, which are located in the contact region I of the f-f 100S dimers, have domains (C-terminal in S9 and R45-H70 in S10) extending to a site close to the probable HPF binding site (Fig. 3, F and G). A conformational change induced

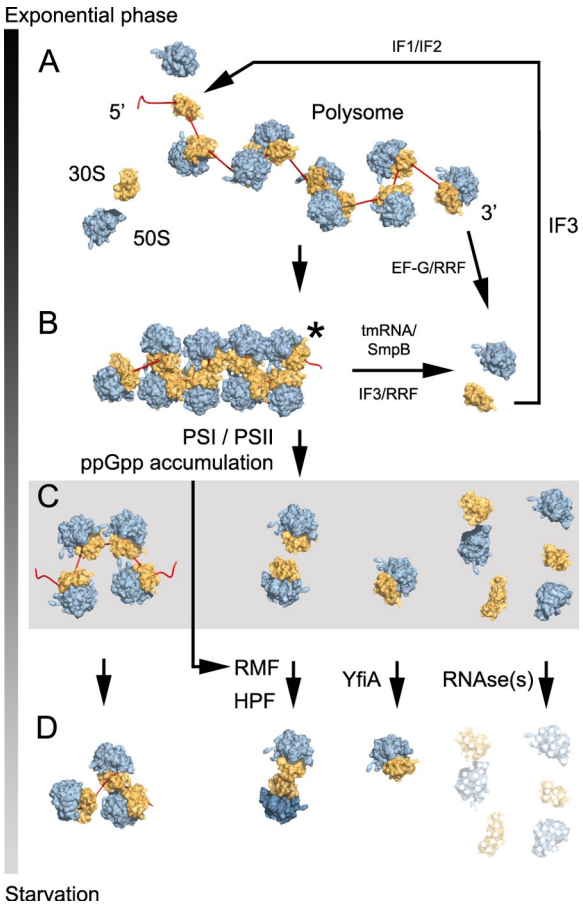

Figure 5. **Model for the changes in ribosomal clustering coupled to growth conditions in *E. coli*.** During transitions from exponential phase (top) to starvation (bottom), relaxed translating polysomes (A) might assume an ordered arrangement (B) when one or more 70S ribosomes become stalled (*). The recycling of ribosomal subunits at canonical stop codons is performed by the EF-G and RRF, while trans-translation (tmRNA/SmpB system) or possible IF3/RRF interactions disassemble stalled ribosomes. In response to nutrient scarcity, empty tRNAs bound to stalled ribosomes induced a stringent response mediated by PSI/PSII, with a consequent accumulation of ppGpp. In turn, this alarmon induces transcription of several genes including the *rmf* gene. RMF inhibit ribosome translation and together with the HPF promote the formation of dimers (D), it is unknown which state of the ribosome (C) is their targets. YfiA binds 70S ribosomes. Endonucleases are responsible for the initial degradation steps of dissociated 50S and 30S ribosomal subunits under starvation, while the 70S and ribosomal dimers likely remain stable.

by HPF or YfiA at the tRNA binding sites could be propagated through the head of the 30S subunit, altering its affinity for another 30S subunit.

Our experiments proved that the 100S ribosome complex is a distinct biologically relevant ribosomal assembly in *E. coli* cells under conditions of nutritional stress. This is in agreement with biochemical studies reporting the appearance of ribosome dimers (Wada, 1998; Ueta et al., 2008). Mutants with a disrupted *rmf* gene do not form ribosome dimers and lose viability earlier than wild-type cells in stationary phase (Yamagishi et al., 1993; Wada et al., 2000). Due to the antagonistic functions of HPF and YfiA, mutants with single deletions in the corresponding genes live slightly longer than wild type (Ueta et al., 2005). These effects on cell survival have been interpreted in terms of ribosome protection against degradation, as the free 50S and

30S subunits, not the 70S particles, are the targets for endoribonuclease action and ultimately degradation (Zundel et al., 2009). Stalled ribosomes can be recovered by the tmRNA system or IF3/RRF interactions causing the release of truncated nascent chains. However, with reduced availability of nutrients, the inactivation of a portion of available ribosomes by RMF/HPF could alleviate the problem of stalling during the transition to stationary phase.

Although active 70S ribosomes are thought to be rare in the stationary phase, the blocking of tRNA binding sites in dimerized ribosomes might allow an effective use of limited aminoacyl-tRNAs for the remaining active ribosomes. Thus, ribosome dimerization might have a dual role in protecting ribosomes against degradation, allowing rapid recovery of translation, and facilitating protein synthesis under stringent conditions by reducing competition for scarce resources (Fig. 5 D). The association of the 100S ribosomes with a variety of factors required for translation may allow these complexes to rapidly resume protein synthesis once more favorable nutrient conditions have been established. Our results provide a model for the interactions of hibernating ribosomes, which can help to direct further biochemical experiments leading to a fuller understanding of the processes underlying their formation.

Materials and methods

Cell cultures

Overnight cultures of *E. coli* (ECOR48) cells in LB medium (0.5 ml) were inoculated into 1 L of medium E (Vogel and Bonner, 1956) supplemented with 2% Bacto-Trypton (Becton Dickinson) and 0.5% glucose at 37°C with shaking at 100 cycles per min during 3 d. These growing conditions are reported to give maximal stationary phase survival for most *E. coli* strains (Wada et al., 2000). For ribosome isolation, cell pellets were stored at −80°C until use. *E. coli* (B/r k) was grown in M9 minimal medium supplemented with 0.03% (wt/vol) alanine (as the sole carbon source) up to mid-exponential and stationary phase (optical density at 600 nm of 0.08 and 0.17, respectively). Cell suspensions were concentrated to an optical density at 600 nm of 0.5 by centrifugation. Stationary phase suspensions were supplemented with 40 µg/ml each amino acid (equi-mass concentration) or LB. For CET, cultures were used immediately after reaching the desired optical density.

Preparation of crude ribosomes

Preparation of crude ribosomes from *E. coli* (ECOR48) or *E. coli* (B/r k) was performed according to the method of Noll et al. (1973) with slight modifications (Horie et al., 1981). Cells were ground with 2.5 volumes of aluminum oxide (type A-5; Sigma-Aldrich) and extracted with buffer I (20 mM Tris-HCl, pH 7.6, 15.2 mM $(CH_3COO)_2Mg$, 0.8 mM EDTA, 100 mM CH_3COONH_4, and 3 mM DTT) containing RNase-free DNase I at 2 µg/ml. Lysates were centrifuged at 18,000 rpm (~30,000 *g*) for 30 min at 4°C on a rotor (model 75Ti; Beckman Coulter). The supernatant was separated on 5 to 20% (wt/vol) sucrose gradients prepared in buffer I. Gradients were centrifuged for 3 h at 40,000 rpm (~275,000 *g*) on a rotor (model SW41 Ti; Beckman Coulter) at 4°C. Elution and fractionation were done from top to bottom and absorbance was recorded at 254 nm. Two pools of fractions, I and II, corresponding to partially overlapping 70S and 100S peaks, respectively, were collected and were dialyzed at 4°C against buffer I to remove the sucrose. A single sucrose gradient was insufficient for the separation of ribosome dimers from monosomes or other complexes, but we avoided further purification steps to prevent possible dissociation of ribosomes.

Mass spectrometry analysis

1 µg crude ribosomal samples were reduced and alkylated (using DTT and iodoacetamide, respectively) and in-solution digested ON using trypsin. The resulting digest was desalted and concentrated on a StageTip followed by speed-vaccing (Rappsilber et al., 2003, 2007). The samples were analyzed on an LTQ-Orbitrap (Thermo Electron) with a nanoPump (model 1100; Agilent Technologies) and an HTC PAL autosampler. The nanoPump delivered a 140-min gradient (5–80% ACN) to a silica emitter packed with a C18-column for reverse-phase separation. Data were acquired using a scan cycle of one full scan MS in the FT (Orbitrap) followed by (up to) six iontrap MS2 scans (LTQ) of the six most intense peaks in the full scan. The acquired MS data were searched against the *E. coli* sequences of SwissProt release 57 using Mascot v 2.2 (Matrix Science) and processed using MaxQuant v1.0.13.13 (Cox and Mann, 2008) with an FDR of 1% (peptide and protein) for the protein list.

Cryoelectron tomography

Dialyzed ribosomal fractions were applied to R2/2 Quantifoil grids (Quantifoil), previously incubated with 10-nm colloidal gold markers. 5 µl of the *E. coli* (B/r k) suspensions were applied to R2/1Quantifoil grids (Quantifoil), followed by 1 µl of colloidal gold (10 nm, protected with BSA). After blotting with filter paper, the grids were vitrified in liquid ethane and stored until usage in liquid nitrogen. For lysates, 26 single-axis tilt series were recorded using a CM20 FEG transmission electron microscope (FEI) operating at 160 kV, a 4096 × 4096 slow-scan CCD camera, and control software for automated image tracking and focusing (TVIPS). The angular range used was ±60°, sampled with angular increments of 3°; and with a cumulative electron dose not exceeding 50 e^- /Å^2. Images were collected using a nominal 3-µm underfocus. The effective magnification was 54,000, which resulted in a pixel size of 0.28 nm for the unprocessed images. Alignment was facilitated by the use of selected gold particles. For 3D reconstruction the images were weighted and back-projected using the TOM software package (Nickell et al., 2005). For cellular CET, tomography data were collected in a cryo-transmission electron microscope (T30 Polara; FEI) equipped with a field emission gun operated at 300 kV. Zero-loss energy filtered images were taken with a 2048 × 2048 Multiscan CCD camera (Gatan) at the end of a GIF 2000 post-column energy filter (Gatan). Tomographs were collected at final magnification of 42105 (giving a pixel size of 0.713 nm at the specimen level) and using a 9 µm underfocus, a tilt range of ±60°, and an angular increment of 1.5°. Alignment and reconstruction were performed using the IMOD software package (Kremer et al., 1996). The number of tomograms analyzed for exponential phase, stationary phase, and aa-supplemented stationary phase was 5, 6, and 4, respectively.

Template matching

For detection of the 70S ribosomes on recorded tomograms, down-sampled reconstructed volumes ([2.24 nm]^3/voxel for tomograms of ribosomal fractions and [1.4] nm]^3/voxel for cellular tomograms) were cross-correlated with a template structure using the program MOLMATCH (Frangakis et al., 2002; Ortiz et al., 2006). The 3D template was generated from 3.5 Å crystal structures of the *E. coli* ribosome (PDB entries 2AW7 and 2AWB; Schuwirth et al., 2005), adjusting pixel size and bandpass filtered to 4 nm (Fig. S1). The cross-correlation function (CCF) was calculated rotating the template over all Euler Angles with 10° increments. A large number of particles *i* with the highest cross-correlation coefficients (CCCs) found were localized in each tomogram extracting the 3D coordinates (x_i, y_i, z_i) and Euler angles (φi, θi, ψ_i) describing the best sampled relative orientation of each particle *i* with respect to the reference. The Eulerian angles φ, θ, and ψ used in this study are defined by clockwise rotations about the z-, x-, and again z-axis of a right-handed static coordinate system x, y, and z, respectively (Nickell et al., 2005; Brandt et al., 2009). These conventions are exemplified with the rotated 70S ribosome map used as reference in Fig. S1.

Averaging and classification of subtomograms

Selected particles were reconstructed in subtomograms with lower binning factor ([0.56 nm]^3/voxel for tomograms of ribosomal fractions and [0.7 nm]^3/voxel for cellular tomograms) and 3D aligned against a 4-nm resolution 70S ribosome reference properly scaled as described previously (Förster et al., 2005; Brandt et al., 2009). 3D alignments and 3D averaging was performed with the use of AV3 (Förster and Hegerl, 2007; Förster et al., 2008). After recognition of putative ribosomes using template matching, subsequent discrimination of false positives was addressed by classification of subvolumes using a constrained-correlation method (Förster et al., 2008) in which the search of similarity between particle pairs was restricted to the volume to be occupied by only one centered ribosome *i*, applying an spherical mask of 14-nm radius. The number of classes was set as high as possible, such that each class contained a small number of particles (at least 20 particles in order to increase the signal of tomograms by one order of magnitude). Averages of classified particles were calculated for each class. Particles contributing to averages not consistent with the ribosome structure were discarded. Thus, 601 particles for tomograms of the Pool I, and 1,232 particles of Pool II, were identified as bona fide ribosomes.

A second step of classification used the same constrained-correlation algorithm but considering only areas surrounding each identified (centered) ribosome *i* in a sphere of 30 nm. Thus, ribosomes pairs with f-f organization were identified. Ribosomes in each dimer with higher similarity to an initial average map were selected to contribute to the same position in the dimer during iterative alignment steps. Thus, 35 dimers (~11% of identified 70S ribosomes) for the Pool I and 28 dimers (~5% of identified 70S ribosomes) from Pool II were averaged.

The analysis of the relative spatial relationship between particles was performed as previously for polysomes (Brandt et al., 2009) with slight modifications. In brief, distances between the center of mass of each detected ribosome *i* and its nearest neighbor *j* were calculated. A vector for ribosome *i* was calculated relative to the coordinates of the reference. Relative euclidic distances and relative angles were hierarchically clustered, using the sum of pairwise dot products as metric. The relative angles were transformed into quaternion space before calculating dot products between pairs of quaternions and back-transformed into Eulerian space for display of clustered rotations. In an alternative classification approach to the constrained-correlation based, we classified particles using this hierarchically clustering of relative localization and orientation.

Resolution of density maps were determined by Fourier shell correlation of two averages each derived of half of the pertinent particles.

Reference-free alignment

The subset of 601 particles from Pool I were aligned in a completely unsupervised manner using a novel, reference-free maximum-likelihood refinement algorithm for 3D images with missing data regions in Fourier space (Scheres et al., 2009). Precentered particles were windowed to 60 × 60 × 60 voxels in order to contain a single ribosome at the center of each particle. An unbiased initial model for the iterative maximum-likelihood refinement algorithm was obtained by assigning random orientations to all particles, resulting in a relatively featureless blob of density. This model was refined during 12 iterations with an angular sampling rate of 12 degrees, followed by 3 more iterations with an angular sampling rate of 9 degrees and restricting the integrations over the angles by ±32 degrees around the optimal angles from the 12th iteration.

Reference-free classification

Unsupervised classification was done using the same 3D maximum likelihood approach, but using the particles without windowing. Unbiased starting models were generated by calculating the average of three random subsets of the particles in random orientations. The resulting models were refined simultaneously against the entire dataset during 25 iterations and using an angular sampling rate of 15 degrees. During the first 5 iterations similarity between the three references was imposed as described previously (Scheres et al., 2009). A smaller spread of ribosome dimer orientations could also be obtained by subsequent reclassification of the dimer class into three subclasses using the same unsupervised maximum likelihood approach. To speed up these calculations all particles were downscaled inside the maximum likelihood program to 40 × 40 × 40 voxels (corresponding to a voxel size of 0.84 nm).

CTF correction

Projection images were aligned (Nickell et al., 2005) and Periodogram averaging (Fernández et al., 1997) was extended over these aligned images resulting in a mean power spectrum for each tilt series (Fernández et al., 2006). The mean power spectrum was filtered (van Heel et al., 2000) to improve the visibility of the Thon rings. Then, the mean defocus was measured using an interactive program written in MATLAB. Assuming an eucentric tilt series we calculated the defocus value for each pixel of the projection images from the mean defocus (Fernández et al., 2006). Defocus correction was done by dividing the projection images in tiles of size 32 × 32 pixels. Boxes with size 256 × 256 pixels containing the tiles were extracted and CTF-corrected by phase flipping using the defocus value of the central pixel of each tile (Zanetti et al., 2009). The corrected tiles were then assembled to the CTF-corrected tilt series.

Fitting of high resolution structures

Fitting was performed in a quantitative manner using Chimera (Pettersen et al., 2004). Docked crystal structures were derived from Protein Data Bank (PDB), entries 2AW7 and 2AWB (Schuwirth et al., 2005), or 1VOQ and 1VOR (Vila-Sanjurjo et al., 2004). For 3D visualization, the programs Chimera (Pettersen et al., 2004) and 3ds max (Discreet) were used.

Accession numbers

The 3D density map of the 100S ribosome in conformation f-f has been deposited in the Electron Microscopy Data Bank with accession code EMD-1750.

Online supplemental material

Fig. S1 shows the orientation conventions used in this study. Fig. S2 is the complete analysis of spatial relationship of in situ identified ribosomes. Fig. S3 shows the resolution improvements gained by CTF correction applied to in vitro data. Fig. S4 shows subsequent unsupervised classification of previously identified ribosome dimers. Table S1 lists the identified protein in crude ribosomal fractions form starved *E. coli* cells. Online supplemental material is available at http://www.jcb.org/cgi/content/full/jcb.201005007/DC1.

We thank S. Etchells and K. Bopp for experimental help at initial steps of the project, T. den Blaauwen for providing us with the *E. coli* strain B/r K, and E. Villa, F. Foerster and D. Thomas for critical reading of the manuscript.

This work received funding from the European Commission's seventh Framework Program (grant agreement HEALTH-F4-2008-201648/PROSPECTS), the Center for Integrated Protein Science Munich (CIPSM), by "Fondation Fourmentin Guilbert", and by a Marie Curie Excellence Grant.

Submitted: 3 May 2010
Accepted: 26 July 2010

References

Brandt, F., S.A. Etchells, J.O. Ortiz, A.H. Elcock, F.U. Hartl, and W. Baumeister. 2009. The native 3D organization of bacterial polysomes. *Cell.* 136:261–271. doi:10.1016/j.cell.2008.11.016

Bremer, H., and P. Dennis. 2008. Feedback control of ribosome function in *Escherichia coli*. *Biochimie.* 90:493–499. doi:10.1016/j.biochi.2007.10.008

Buchan, J.R., and I. Stansfield. 2007. Halting a cellular production line: responses to ribosomal pausing during translation. *Biol. Cell.* 99:475–487. doi:10.1042/BC20070037

Cox, J., and M. Mann. 2008. MaxQuant enables high peptide identification rates, individualized p.p.b.-range mass accuracies and proteome-wide protein quantification. *Nat. Biotechnol.* 26:1367–1372. doi:10.1038/nbt.1511

Fernández, J.J., J.R. Sanjurjo, and J.M. Carazo. 1997. A spectral estimation approach to contrast transfer function detection in electron microscopy. *Ultramicroscopy.* 68:267–295. doi:10.1016/S0304-3991(97)00032-6

Fernández, J.J., S. Li, and R.A. Crowther. 2006. CTF determination and correction in electron cryotomography. *Ultramicroscopy.* 106:587–596. doi:10.1016/j.ultramic.2006.02.004

Förster, F., and R. Hegerl. 2007. Structure determination in situ by averaging of tomograms. *Methods Cell Biol.* 79:741–767. doi:10.1016/S0091-679X(06)79029-X

Förster, F., O. Medalia, N. Zauberman, W. Baumeister, and D. Fass. 2005. Retrovirus envelope protein complex structure *in situ* studied by cryo-electron tomography. *Proc. Natl. Acad. Sci. USA.* 102:4729–4734. doi:10.1073/pnas.0409178102

Förster, F., S. Pruggnaller, A. Seybert, and A.S. Frangakis. 2008. Classification of cryo-electron sub-tomograms using constrained correlation. *J. Struct. Biol.* 161:276–286. doi:10.1016/j.jsb.2007.07.006

Frangakis, A.S., J. Böhm, F. Förster, S. Nickell, D. Nicastro, D. Typke, R. Hegerl, and W. Baumeister. 2002. Identification of macromolecular complexes in cryoelectron tomograms of phantom cells. *Proc. Natl. Acad. Sci. USA.* 99:14153–14158. doi:10.1073/pnas.172520299

Horie, K., A. Wada, and H. Fukutome. 1981. Conformational studies of *Escherichia coli* ribosomes with the use of acridine orange as a probe. *J. Biochem.* 90:449–461.

Izutsu, K., A. Wada, and C. Wada. 2001. Expression of ribosome modulation factor (RMF) in *Escherichia coli* requires ppGpp. *Genes Cells.* 6:665–676. doi:10.1046/j.1365-2443.2001.00457.x

Kato, T., H. Yoshida, T. Miyata, Y. Maki, A. Wada, and K. Namba. 2010. Structure of the 100S ribosome in the hibernation stage revealed by electron cryomicroscopy. *Structure.* 18:719–724. doi:10.1016/j.str.2010.02.017

Kremer, J.R., D.N. Mastronarde, and J.R. McIntosh. 1996. Computer visualization of three-dimensional image data using IMOD. *J. Struct. Biol.* 116:71–76. doi:10.1006/jsbi.1996.0013

Lučić, V., F. Förster, and W. Baumeister. 2005. Structural studies by electron tomography: from cells to molecules. *Annu. Rev. Biochem.* 74:833–865. doi:10.1146/annurev.biochem.73.011303.074112

Maki, Y., H. Yoshida, and A. Wada. 2000. Two proteins, YfiA and YhbH, associated with resting ribosomes in stationary phase *Escherichia coli. Genes Cells.* 5:965–974. doi:10.1046/j.1365-2443.2000.00389.x

Marzi, S., A.G. Myasnikov, A. Serganov, C. Ehresmann, P. Romby, M. Yusupov, and B.P. Klaholz. 2007. Structured mRNAs regulate translation initiation by binding to the platform of the ribosome. *Cell.* 130:1019–1031. doi:10.1016/j.cell.2007.07.008

Murray, K.D., and H. Bremer. 1996. Control of spoT-dependent ppGpp synthesis and degradation in *Escherichia coli. J. Mol. Biol.* 259:41–57. doi:10.1006/jmbi.1996.0300

Nickell, S., F. Förster, A. Linaroudis, W.D. Net, F. Beck, R. Hegerl, W. Baumeister, and J.M. Plitzko. 2005. TOM software toolbox: acquisition and analysis for electron tomography. *J. Struct. Biol.* 149:227–234. doi:10.1016/j.jsb.2004.10.006

Noll, M., B. Hapke, M.H. Schreier, and H. Noll. 1973. Structural dynamics of bacterial ribosomes. I. Characterization of vacant couples and their relation to complexed ribosomes. *J. Mol. Biol.* 75:281–294. doi:10.1016/0022-2836(73)90021-1

Ortiz, J.O., F. Förster, J. Kürner, A.A. Linaroudis, and W. Baumeister. 2006. Mapping 70S ribosomes in intact cells by cryoelectron tomography and pattern recognition. *J. Struct. Biol.* 156:334–341. doi:10.1016/j.jsb.2006.04.014

Pettersen, E.F., T.D. Goddard, C.C. Huang, G.S. Couch, D.M. Greenblatt, E.C. Meng, and T.E. Ferrin. 2004. UCSF Chimera—a visualization system for exploratory research and analysis. *J. Comput. Chem.* 25:1605–1612. doi:10.1002/jcc.20084

Rappsilber, J., Y. Ishihama, and M. Mann. 2003. Stop and go extraction tips for matrix-assisted laser desorption/ionization, nanoelectrospray, and LC/MS sample pretreatment in proteomics. *Anal. Chem.* 75:663–670. doi:10.1021/ac026117i

Rappsilber, J., M. Mann, and Y. Ishihama. 2007. Protocol for micro-purification, enrichment, pre-fractionation and storage of peptides for proteomics using StageTips. *Nat. Protoc.* 2:1896–1906. doi:10.1038/nprot.2007.261

Sato, A., T. Watanabe, Y. Maki, M. Ueta, H. Yoshida, Y. Ito, A. Wada, and M. Mishima. 2009. Solution structure of the *E. coli* ribosome hibernation promoting factor HPF: Implications for the relationship between structure and function. *Biochem. Biophys. Res. Commun.* 389:580–585. doi:10.1016/j.bbrc.2009.09.022

Scheres, S.H., R. Melero, M. Valle, and J.M. Carazo. 2009. Averaging of electron subtomograms and random conical tilt reconstructions through likelihood optimization. *Structure.* 17:1563–1572. doi:10.1016/j.str.2009.10.009

Schmeing, T.M., and V. Ramakrishnan. 2009. What recent ribosome structures have revealed about the mechanism of translation. *Nature.* 461:1234–1242. doi:10.1038/nature08403

Schuwirth, B.S., M.A. Borovinskaya, C.W. Hau, W. Zhang, A. Vila-Sanjurjo, J.M. Holton, and J.H.D. Cate. 2005. Structures of the bacterial ribosome at 3.5 A resolution. *Science.* 310:827–834. doi:10.1126/science.1117230

Singh, N.S., R. Ahmad, R. Sangeetha, and U. Varshney. 2008. Recycling of ribosomal complexes stalled at the step of elongation in *Escherichia coli. J. Mol. Biol.* 380:451–464. doi:10.1016/j.jmb.2008.05.033

Tissieres, A., and J.D. Watson. 1958. Ribonucleoprotein particles from *Escherichia coli. Nature.* 182:778–780. doi:10.1038/182778b0

Ueta, M., H. Yoshida, C. Wada, T. Baba, H. Mori, and A. Wada. 2005. Ribosome binding proteins YhbH and YfiA have opposite functions during 100S formation in the stationary phase of *Escherichia coli. Genes Cells.* 10:1103–1112. doi:10.1111/j.1365-2443.2005.00903.x

Ueta, M., R.L. Ohniwa, H. Yoshida, Y. Maki, C. Wada, and A. Wada. 2008. Role of HPF (hibernation promoting factor) in translational activity in *Escherichia coli. J. Biochem.* 143:425–433. doi:10.1093/jb/mvm243

van Heel, M., B. Gowen, R. Matadeen, E.V. Orlova, R. Finn, T. Pape, D. Cohen, H. Stark, R. Schmidt, M. Schatz, and A. Patwardhan. 2000. Single-particle electron cryo-microscopy: towards atomic resolution. *Q. Rev. Biophys.* 33:307–369. doi:10.1017/S0033583500003644

Vila-Sanjurjo, A., B.S. Schuwirth, C.W. Hau, and J.H. Cate. 2004. Structural basis for the control of translation initiation during stress. *Nat. Struct. Mol. Biol.* 11:1054–1059. doi:10.1038/nsmb850

Vogel, H.J., and D.M. Bonner. 1956. Acetylornithinase of *Escherichia coli*: partial purification and some properties. *J. Biol. Chem.* 218:97–106.

Wada, A. 1998. Growth phase coupled modulation of *Escherichia coli* ribosomes. *Genes Cells.* 3:203–208. doi:10.1046/j.1365-2443.1998.00187.x

Wada, A., Y. Yamazaki, N. Fujita, and A. Ishihama. 1990. Structure and probable genetic location of a "ribosome modulation factor" associated with 100S ribosomes in stationary-phase *Escherichia coli* cells. *Proc. Natl. Acad. Sci. USA.* 87:2657–2661. doi:10.1073/pnas.87.7.2657

Wada, A., K. Igarashi, S. Yoshimura, S. Aimoto, and A. Ishihama. 1995. Ribosome modulation factor: stationary growth phase-specific inhibitor of ribosome functions from *Escherichia coli. Biochem. Biophys. Res. Commun.* 214:410–417. doi:10.1006/bbrc.1995.2302

Wada, A., R. Mikkola, C.G. Kurland, and A. Ishihama. 2000. Growth phase-coupled changes of the ribosome profile in natural isolates and laboratory strains of *Escherichia coli. J. Bacteriol.* 182:2893–2899. doi:10.1128/JB.182.10.2893-2899.2000

Woldringh, C.L., M.A. de Jong, W. van den Berg, and L. Koppes. 1977. Morphological analysis of the division cycle of two *Escherichia coli* substrains during slow growth. *J. Bacteriol.* 131:270–279.

Yamagishi, M., H. Matsushima, A. Wada, M. Sakagami, N. Fujita, and A. Ishihama. 1993. Regulation of the *Escherichia coli* rmf gene encoding the ribosome modulation factor: growth phase- and growth rate-dependent control. *EMBO J.* 12:625–630.

Yoshida, H., Y. Maki, H. Kato, H. Fujisawa, K. Izutsu, C. Wada, and A. Wada. 2002. The ribosome modulation factor (RMF) binding site on the 100S ribosome of *Escherichia coli. J. Biochem.* 132:983–989.

Yoshida, H., H. Yamamoto, T. Uchiumi, and A. Wada. 2004. RMF inactivates ribosomes by covering the peptidyl transferase centre and entrance of peptide exit tunnel. *Genes Cells.* 9:271–278. doi:10.1111/j.1356-9597.2004.00723.x

Yoshida, H., M. Ueta, Y. Maki, A. Sakai, and A. Wada. 2009. Activities of *Escherichia coli* ribosomes in IF3 and RMF change to prepare 100S ribosome formation on entering the stationary growth phase. *Genes Cells.* 14:271–280. doi:10.1111/j.1365-2443.2008.01272.x

Yusupova, G., L. Jenner, B. Rees, D. Moras, and M. Yusupov. 2006. Structural basis for messenger RNA movement onthe ribosome. *Nature*. 444:391–394. doi:10.1038/nature05281

Zanetti, G., J.D. Riches, S.D. Fuller, and J.A. Briggs. 2009. Contrast transfer function correction applied to cryo-electron tomography and sub-tomogram averaging. *J. Struct. Biol.* 168:305–312. doi:10.1016/j.jsb.2009.08.002

Zundel, M.A., G.N. Basturea, and M.P. Deutscher. 2009. Initiation of ribosome degradation during starvation in *Escherichia coli*. *RNA*. 15:977–983. doi:10.1261/rna.1381309